Title

RECRYSTALLIZATION OF BURIED AMORPHOUS LAYERS AND ASSOCIATED ELECTRICAL EFFECTS IN P+ IMPLANTED Si

Authors

Sadana, D.K.
Washburn, J.
Booker, G.R.

Publication Date

1982-08-01

LBL-14889
Preprint

Lawrence Berkeley Laboratory
UNIVERSITY OF CALIFORNIA

Materials & Molecular
Research Division

Submitted to Philosophical Magazine

RECRYSTALLIZATION OF BURIED AMORPHOUS LAYERS AND ASSOCIATED ELECTRICAL EFFECTS IN P^+ IMPLANTED Si

D.K. Sadana, J. Washburn, and G.R. Booker

August 1982

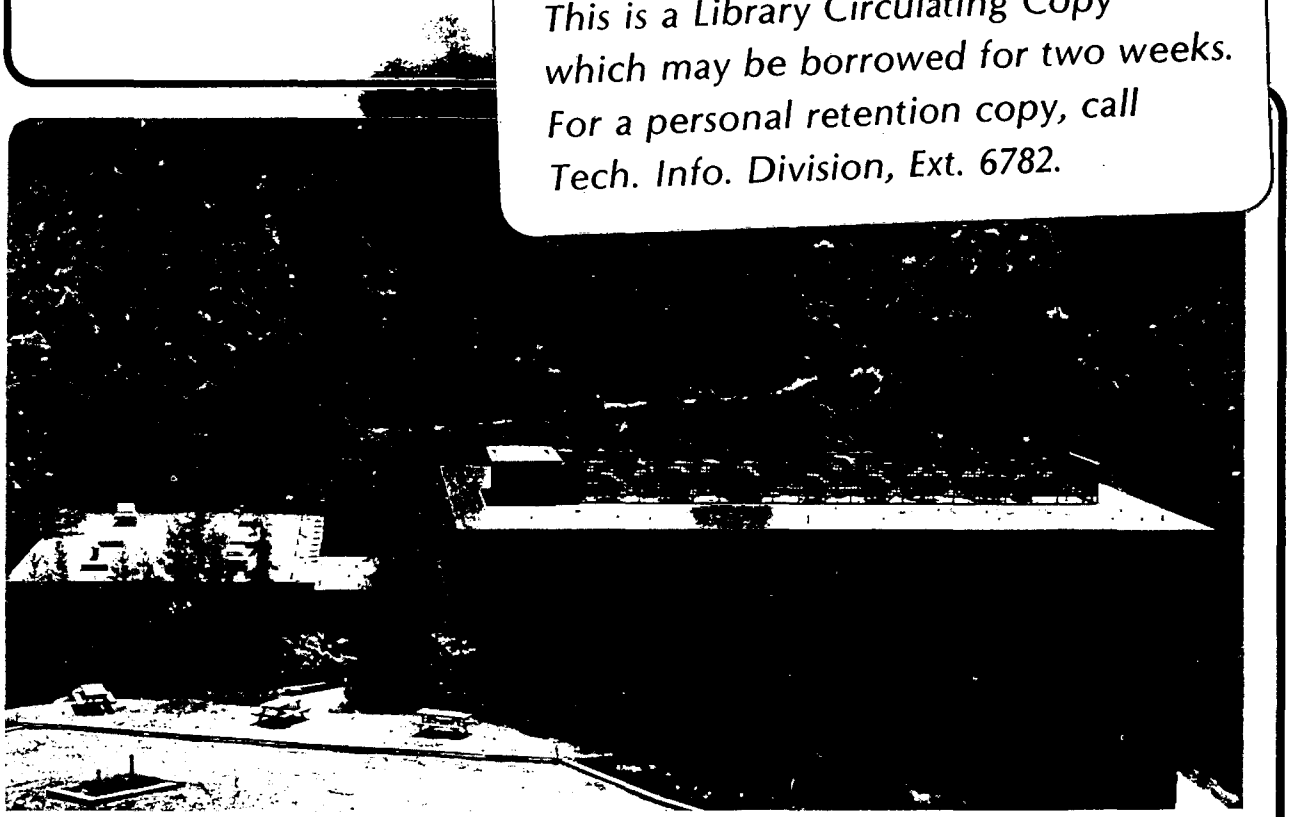

Prepared for the U.S. Department of Energy under Contract DE-AC03-76SF00098

DISCLAIMER

RECRYSTALLIZATION OF BURIED AMORPHOUS LAYERS AND ASSOCIATED ELECTRICAL EFFECTS IN P^+ IMPLANTED Si

D. K. Sadana and J. Washburn
Lawrence Berkeley Laboratory
University of California
Berkeley, CA 94720

and

G. R. Booker
Department of Metallurgy and Materials Science
University of Oxford
Oxford, OX 1 3PH (England)

ABSTRACT

Recrystallization behaviour of a buried amorphous layer formed due to P^+ implantation into (111)Si has been studied using transmission electron microscopy (TEM), secondary ion mass spectroscopy (SIMS) and Hall measurements. Special TEM specimen preparation techniques were used to study individual sub-surface damage regions in the as-implanted as well as the annealed samples. The TEM results showed that the recrystallization of the amorphous layer began slowly, increased rapidly above 550°C and was complete at 600°C. At temperatures $\geq$750°C $\leq$ 1000°C, two discrete layers of interstitial a/2 <110> and a/3 <111> dislocation loops formed below the specimen surface and the surface region contained stacking fault tetrahedra. The SIMS results showed that pronounced segregation of phosphorus atoms occcurred in the defects rich regions at 750°C. At higher annealing temperatures, P segregation still occurred, but the magnitude of the segregation reduced because of the diffusive effects. The segregation results correlated with the asymmetry in the inside/outside diffraction

contrast results of the dislocation loops. The asymmetry was maximum in the 750°C annealed specimen and decreased progressively with increasing annealing temperature. Electrical profiles showed decreases in carrier concentration and/or mobility at the defects rich regions.

INTRODUCTION

When impurity atoms are introduced into randomly oriented single crystal Si by ion implantation (up to energies of 500 kV), the depth distribution of the introduced atoms as well as the damage caused by their knock-on collisions with the host Si atoms is gaussian. The peak of the damage distribution has been found to precede the peak of the implanted atoms distribution (Rp) by a factor of 0.7 [Crowder and Title, 1970]. When the dose and implantation temperature are low ($\leq 10^{13}$ cm^{-2}, 77°K), the damage created by each individual ion appears as a small damage cluster ($\leq$20 Å across) in a transmission electron microscope (TEM) and the density of these clusters peaks at ~0.7 Rp [Sadana, unpublished]. Consequently, when the implantation dose is increased, the overlapping of the small damage clusters first create a buried amorphous layer at a mean depth of 0.7 Rp. Further increase n the dose causes broadening of the amorphous layer such that it extends to the surface. The broadening about the damage maximum at 0.7 Rp is asymmetric, being greater towards the surface. This is because of higher total displacement damage near the surface than that in the deeper parts.

Understanding of the recrystallization behaviour of these various types of damage structure caused by different ions on subsequently furnace annealing has been the subject of study for the last two decades [Csepregi et al., 1977; Chadderton and Eisen, 1971; Washburn, 1981; Davidson and Booker, 1970; Bicknell, 1973; Lau, 1978; Tseng et al., 1976; Komarov et al., 1979; Gerasimov et al., 1972; Csepregi

et al., 1975]. In most of the cases reported in the literature, the initial damage distribution was such that the amorphous layer extended to the surface. Detailed TEM and MeV He^+ channeling/Rutherford backscattering (RBS) studies on annealing of these layers showed that the amorphous material in the implanted region regrows on the underlying single crystal Si by solid phase epitaxy. Different types of secondary defects, such as dislocation loops, twins, line dislocations, stacking faults, etc., have been found to nucleate at the amorphous/crystalline interface and/or within the damage region [Madden, 1974; Fletcher and Booker, 1978]. On the basis of recently performed in situ TEM annealing experiments, the formation and migration of microtwins on the {111} planes in ion implanted (111)Si as well as the orientation dependence of amorphous/crystalline migration rates were successfully explained by Drosd and Washburn [1981, 1982] by considering atomic bonding arrangements at the amorphous/crystalline interface. Similar theoretical model has also been developed by Spaepan [1978].

However, a detailed recrystallization study of buried amorphous layers is still lacking. In this paper, furnace annealing results of a buried amorphous layer produced by P^+ implantation into (111) Si have been described. A combination of techniques including TEM, secondary ion mass spectroscopy (SIMS) and electrical measurements was used for this study. Extensive TEM examinations were carried out on both plan and cross-section specimens annealed in the temperature range 400-1050°C to obtain spatial as well as the depth distributions of defects. It was found that annealing at or above 650°C gives rise to

the formation of two discrete damage layers containing dislocation loops. In order to obtain detailed TEM information from individual damage layers, special TEM specimen preparation methods were used (see Section B under Experimental).

Previous workers have also obtained evidence for such double damage layers in ion implanted Si samples. Masters et al. [1970] using a radiochemical method in conjunction with copper decoration, found two discrete peaks when they measured copper concentration as a function of depth for Si implanted at room temperature with 10^{16} cm^{-2} of 125 KeV P^+ ions. Cspregi et al. [1976], using the MeV He^+ channeling method, found two disorder peaks for Si implanted at above room temperature with 10^{16} cm^{-2} of 125 KeV P^+ ions. However, it is believed that the present work represents the first detailed study of such double damage layers by using cross-section TEM specimens.

There is considerable interest in correlating ion implantation damage with electrical effects. To understand the effect of damage on electrical properties it is important to know how the implanted impurity redistribute itself near the defects on subsequent furnace annealing and then compare structural profiles with electrical profiles, profile being taken to mean information as a function of depth. The atomic and electrical profiles in this study were obtained by SIMS and Hall measurements in conjunction with low voltage ($\leq$6 kV) ion-beam stripping. To make valid comparisons, the latter measurments were performed on the adjacent regions of the same samples used for the TEM analyses. Strong correlations between ion damage, impurity, segregation, and electrical properties were observed [Sadana et al., 1977].

EXPERIMENTAL

A. Implantation

The starting material was B doped 10 ohm cm (111) Si polished on one side. Samples were blanket implanted on the polished side at room temperature in a non-channelling direction with 5×10^{14} cm^{-2} p^+ ions at 120 keV corresponding to an LSS mean projected range Rp of 1490 ± 410 Å. The estimated rise in the surface temperatures during the implantation was ~80°C. Some samples were not annealed while other individual samples were subsequently annealed in a nitrogen atmosphere at a particular temperature for 20 minutes, the temperatures selected being 400, 550, 650, 750, 850, 950, 1000, and 1050°C.

B. TEM Specimen Preparation

The implanted samples were jet chemically thinned using HNO_3/HF from the unimplanted side only to give plan-view specimens. Other samples were cleaved, mechanically polished and ion-beam thinned (50 μA at 6 kV) from both sides to produce 90° cross-section specimens using the method of Pettit and Booker [1971]. In general, the plan-view specimens proved to be better for determining the nature of the damage, while the cross-section specimens were better for determining the depth distributions. However, in order to carry out a detailed TEM investigation of the damage in the surface region and that in the sub-surface regions, plan view specimens were used and the procedure adopted is described in Figs. 1 and 2.

For all of the cross-section specimens (unannealed -1050°C annealed) and some of the plan view specimens (unannealed -550°C annealed), TEM examinations were performed by tilting the specimens to give two-beam

bright-field diffraction conditions for either a 111 or 220 type reflection. Transmission electron diffraction patterns (TED) were also obtained from the individual damage regions either from plan-view specimens, as described in Fig. 1, or directly from cross-section specimens by operating Philips EM400 in the convergent beam diffraction mode. For the plan view specimens annealed at or above 750°C, weak beam diffraction conditions for a 220 type reflection or {111} type reflection were used.

C. Electrical Profiles

Carrier concentration and mobility depth profiles were obtained from some of the annealed samples using van der Pauw method in conjunction with ion beam milling [Davidson, 1972]. The mobility has been plotted as the ratio of the determined mobility (μ) and the mobility taken from the data of Irvin corresponding to the determined carrier concentration (Fig. 20). The procedure was used to eliminate the effect of the variation in the dopant concentration within the implanted region on the shape of the mobility-profile.

D. Atomic Profiles

The depth distribution of P atoms was obtained by secondary ion mass spectroscopy (SIMS). The SIMS measurements were performed with a Cs^+ primary ion bombardment and negative secondary ion beam detection in ultra high vacuum of $<10^{-10}$ Torr [Magee, 1979].

RESULTS

A. TEM: Unannealed to 550°C (Cross-Sections)

A typical micrograph from cross-section specimen corresponding to the unannealed sample is shown in Fig. 3a. A buried amorphous layer of thickness 1350 Å occurred. The micrograph also revealed that both

the upper and lower amorphous/crystalline interfaces were irregular and there was significant interpenetration of amorphous and crystalline regions at the interfaces. Undulations with amplitude up to 150 Å measured perpendicular to the specimen surface occurred. There was also evidence of the presence of a small density of randomly distributed microcrystallites ($\leq$ 50 Å across) within the amorphous layer (small dark dots in region Q, Fig. 3a). This was confirmed by convergent beam TED patterns from the individual regions P, Q and R of the same specimen shown in Fig. 5. The patterns were taken from specimen areas ~200 Å in diameter. The presence of a strong undiffracted and diffracted spots in the patterns from regions P and R shows that the material in both of these regions was single crystal. On the other hand, the pattern from region Q showed only a strong undiffracted spot and very faint diffracted spots (not clearly visible in the figure) indicating that this material was almost amorphous but not entirely and contained minute quantity of crystalline material. It should be noted that the diffraction spots in the TED from region Q were located exactly at the positions where the spots from regions P and R were located. This indicates that the microcrystals within the amrophous matrix are not randomly oriented, but retain the original substrate orientation. A thin wedge shaped region of this specimen showed thickness fringes running across the various interfaces to the specimen surface. Such fringes were well-defined in regions P and R but were not detectable in region Q, because these fringes arose from diffraction contrast. Their behaviour supported the view that regions P and R were single crystal, and region Q was primarily amorphous. Moreover,

the change from fringes to no fringes on going from crystalline to amorphous material took place relatively abruptly.

Micrographs from cross-section specimens corresponding to 400° and 550°C anneals are shown in Fig. 3b and 3c, respectively. As the annealing temperature was increased, the recrystallization of the amorphous layer began slowly, increased rapidly above 550°C and was complete at 600°C. For example, at 400°C the amorphous layer was 920 Å thick, and for 550°C, it was 750 Å thick. However, the recrystallization in this temperature range proceeded mainly from the lower amorphous/crystalline interface (Fig. 3). For 650°C, no amorphous layer remained (see Section C). For the 550°C specimen, an additional band of fine defects was present below the buried amorphous layer at a mean depth of 2250 Å. The position of this fine defect band in the 550°C specimen corresponded to the region just below the second amorphous/crystalline interface in the unannealed specimen. The latter is the region in the unannealed specimen where the material although still single crystal, is heavily damaged. The amorphous layer appeared dark in the bright field micrographs because a large fraction of the incident electrons were scattered outside the contrast aperture of the electron microscope within the layer than was the case for the surrounding crystalline material. The microdiffraction and fringe contrast results from 400° to 550°C specimens were similar to that obtained for the unannealed sample.

B. TEM: Unannealed to 550°C (Plan-Views)

Micrographs from plan view specimens corresponding to no annealing are shown in Fig. 5. The micrograph of Fig. 5a was obtained as

illustrated in Fig. 1b. The left side of the micrograph corresponded to area A1 (material in the region P) and the selected-area TED pattern consisted of a single crystal spot pattern. The right side corresponded to area A2 (materials from regions P and Q), and the pattern was now similar but contained in addition amorphous rings. The micrograph of Fig. 5b was obtained as illustrated in Fig. 1c. The left side corresponded to area B1 (material in the region Q), and the pattern consisted of amorphous rings. The right side corresponds to area B2 (material in the regions Q and R), and the pattern was now similar but contained in addition single crystal spots. The micrograph of Fig. 5c was obtained as illustrated in Fig. 1d. The whole micrograph corresponds to region C1. The fine dotty structure of region A2 corresponded to fine damage present immediately above the buried amorphous band, while the coarse dotty structure of regions A3 and B2 corresponded to corase damage that was present immediately below the buried amorphous band. Similar results were obtained for 400° and 550°C annealed specimens (micrographs not included in the text).

C. TEM: Annealed 650° to 1050°C (Cross-Sections and Plan-Views)

Micrographs from cross-section and plan-view specimens corresponding to a 650° anneal are shown in Fig. 6. TED studies showed that no amorphous material remained. The cross-section micrograph showed a first damage layer at a mean depth of 1270 Å and a second at 2250 Å. The first layer was well-defined, while the second consisted of fine defects. Examination of plan-view micrographs using the procedure of Fig. 2b showed that loops up to ~1000 Å across and fine damage ($\leq$50 Å) occurred in the first damage layer, while the fine damage only occurred in the second damage layer.

Micrographs from cross-section and plan-view specimens corresponding to 750°C anneal are shown in Fig. 7. The cross-section micrograph (Fig. 7a) shows two well defined layers at mean depths of 1200 Å and 2000 Å, the first layer containing larger dislocation loop defects. Plan-view micrographs were obtained using the procedure of Fig. 2 such that Fig. 7b corresponded to area A2 of Fig. 2b and Fig. 7c corresponds to area B2 of Fig. 2c, i.e., the two damage layers were now separated in the two plan view micrographs consequently, examination and identification of the defect in the two layers could be better performed. In addition to the dislocation loops in the two layers, there was a high density of stacking fault tetrahedra (SFTs) in the region between the surface and first damage layer. The data concerning these defects is given in Table 2. The analysis of these defects indicated that the first layer contained the loops with a/2 <110> type Burgers vectors and the loops lay along three shallowly inclined {110} planes (35° with respect to the surface). The loops showing milky contrast had Burgers vectors of a/3 <111> type and these lay on a (111) plane parallel to the plane of the implanted surface [Jenkins et al., 1973]. The second layer also contained similar types of loops, however, three inclined a/3 <111> type loops were also present. All of the loops were extrinsic and corresponded to extra planes of atoms inside the loop (data, Table 2). From the dislocation loops density and their habit planes data, the total number of atoms in the extra half planes of the loops was determined to be 8.2×10^{14} cm^{-2}.

Micrographs from cross-section and plan-view specimens corresponding to 850°C and 950°C anneals are shown in Figs. 8 and 1. The cross-section micrographs again showed two well defined damage layers, with each layer containing dislocation loops. The results obtained were similar to that obtained for the 750°C specimen. However, as the annealing temperature increased, the loops in the two damage layers became larger and less numerous, and also better defined in shapes (data, Table 2). The number of atoms in the extra half planes of the loops in the 850°C and 950°C annealed sampler was determined to be 2.6 x 10^{15} cm^{-2} and 4.3 x 10^{14} cm^{-2}, respectively.

Micrographs from cross-section and plan-view specimen corresponding to a 1050°C anneal are shown in Fig. 10. The cross-section micrograph showed that the second damage layer had completely annealed out, while the loops in the first damage layer were still present. The relative average sizes of the inclined a/2 <110> and parallel a/3 <111> type loops compared with the loops in 950°C anneal had increased by a factor of ~X4 and numerous SFTs were present between the specimen surface and damage layer (data, Table 2). The number of atoms associated with the loops in this case was 6.6 x 10^{15} cm^{-2}, i.e., ~13 times more than the implanted dose.

D. SIMS (Unannealed-950°C)

The P profile from the implanted but unannealed sample showed a gaussian distribution with a peak at 1500 Å from the surface. The position of the peak was in agreement with the theoretically predicted LSS range (Rp). A deep tail extending to a depth of ~X3 Rp was present in the SIMS profile. There was no significant change in the

shapes of the profiles from the samples annealed up to 650°C (Fig. 11) as compared to that of the unannealed sample. However, the profile from a 750°C annealed sample showed a remarkable redistribution of P atoms (Fig. 12). It showed a hump and a sharp peak at depths of 700 Å and 1100 Å, respectively, a nearly flat concentration distribution over the depth range of 1100 to 1750 Å, followed by a sharp drop at a depth of 2200 Å. There was a considerable 'swelling' of P profile in the deeper parts (Fig. 12). The profile from an 850°C annealed sample again changed significantly from the 750°C sample. It showed segregation of P atoms at depths of 1100 Å and 1700 Å (see the humps in the profiles, Fig. 13). In addition, a significant amount of P diffusion was observed both toward the surface as well as deeper (~X4 Rp) into the material. The profile from a 950°C annealed sample showed further broadening of the gaussian peak and a still deeper tail as expected.

E. Asymmetric Diffraction Contrast - SIMS Correlations

The inside/outside diffraction contrast from a "pure" dislocation loop is known to be symmetrical about the dislocation cores [Hirsch et al., 1965]. Segregation of impurities at preferred crystallographic sites around a dislocation loop can make the inside/outside contrast of a loop unsymmetrical. From the depth distributions of the dislocation loops (Figs. 7, 8 and 9) and P atoms (Figs. 12, 13 and 14) for the samples annealed at 750°C, 850°C and 950°C, it is clear that a large concentration of P atoms are present in the vicinity of the dislocation loops. Whether or not these atoms are near the dislocation cores can therefore be determined from the inside/outside diffraction contrast

experiments. Figures 15, 16 and 17 show a series of TEM micrographs from the above samples under +g/-g diffraction candidates. The two sets of the dislocation loops showing inside and outside contrasts under +g diffraction conditions have been represented by 'A' and 'B' respectively; and vice versa under -g diffraction condition. It is clear that there is a pronounced asymmetry in the inside/outside contrast of the loops in the 750°C sample (Fig. 15) and that the asymmetry progressively decreases with increasing annealing temperature (Figs. 16 and 17). The concentration of P atoms were 4×10^{19} cm^{-2}, 2.9×10^{19} cm^{-3} and 1.4×10^{19} cm^{-3}, at the first layer of the dislocation loops, and 2.5×10^{19} cm^{-3}, 2×10^{19} cm^{-3} and 1.3×10^{19} cm^{-3} at the second layer of the dislocation loops in 750° and 850° and 950°C samples, respectively.

F. Electrical Measurements: Correlation with Cross-Sectional TEM Results

The carrier concentration (n) profile (Fig. 18) from the 950°C sample showed a pronounced dip at a mean depth of 750 Å and possibly a slight shoulder at 2200 Å. The mobility (μ_r) profile showed two dips at mean depths of 750 Å and 1900 Å. The dip in the n profile occurred slightly above the position of the first damage layer at 1070 Å. The value of n (cm^{-3}) was less by X5 compared with the value of P atoms at this depth. The two dips in the μ_r profile at 750 Å and 1900 Å correlate reasonably well with the positions of the first and second damage layers at 1070 Å and 2100 Å, respectively.

These results indicate that the mobility and carrier concentration are affected in the presence of the defects but the extent of the effect is a complex function of the defect-impurity interaction.

DISCUSSION

I. Formation and Recrystallization of Amorphous Layers

Our TEM results indicate that the single crystal to amorphous transformation in P^+ implanted Si is relatively abrupt. For example, in Fig. 3a there is no evidence of a gradual change in the diffraction contrast from single crystal (regions P and R) to the amorphous region (region Q). The contrast changes from black (amorphous) to white (single crystal) rather abruptly. The occurrence of this phenomenon was also evident in the thin part of the cross-section specimen of Fig. 3a where the thickness fringes in regions P and R terminated abruptly in region Q (micrograph not included in the text).

The distribution of vacancies and interstitials in the implanted region can be predicted by considering simple collision kinetics. When P atoms are introduced into the Si lattice, each collision at the surface is likely to cause vacancies near the surface and interstitials (deflected Si and P atoms) deeper into the material. This is because of the dynamic crowdion action that tends to produce interstitials at some distance from the site of a primary knock-on, while vacancies because they have no means of propagation, remain behind in fairly compact groups [Chadderton, 1965]. At the implantation energy used, a variety of clusters of vacancies and possibly more complex configurations resulting from the collapse or rearrangement of such clusters are expected near the surface. Further clustering of these vacancies should occur on subsequent annealing. It is probably this high concentration of vacancies and their complexes that retards the recrystallization of the amorphous layer at the upper amorphous/crystalline

interface at low ($\leq$550°C) temperatures (Fig. 3). The presence of the vacancies in the near-surface region is further confirmed by the formation of stacking fault tetrahedra (SFTs) in this region. All of the reported work on metals in the literature to authors knowledge indicate that the SFTs represent vacancy clusters, 50-100 Å across [Silcox and Hirsch, 1959; Cottrill, 1961; Saldin et al., 1979]. Unlike in the low temperature annealing case, the vacancies in the near-surface region probably recombine with the interstitials at high annealing temperature and thereby provide a good single-crystal seed at the upper amorphous/crystalline interface. The recrystallization rates under these circumstances are expected to be equal at the two interfaces. Therefore, the first secondary damage layer is caused by the solid state recrystallization of layer "Q" that begins simultaneously both at the upper and lower damage/crystalline interfaces on subsequent annealing at 750°C or above. These oppositely moving interfaces eventually meet each other at the middle of the damage region "Q". The extra Si and P interstitials contained in the damage region coalesce to form the dislocation loops seen as layer "S." The damage in the second layer may result from the implanted atoms that were steered into channeling directions near the end of their implanted trajectories. These form small invisible (by TEM) interstitial clusters at room temperature beyond the main peak of the projected range. Subsequent annealing at 750°C causes these mobile interstitial to cluster together and form small dislocation loops (layer "T").

As the annealing temperature is further increased, the loops in the two damage layers become larger and less numerous and also more geometric in shape. The particular types of loops in the two damage layers are different in that the first damage layer does not have inclined a/3 <111> loops. This suggests that there are directional stresses in the material in this region. The damaged material is under biaxial compression due to the presence of the interstitials and vacancies, and the volume expansion due to the lower density of the amorphous material. The formation of steeply inclined a/3 <111> interstitial loops would increase this internal stress, whereas the formation of either parallel or shallowly inclined loops with respect to the specimen surface would not have a serious effect. Therefore, the expected internal stresses appear to explain the observed behavior. The second damage layer does have inclined a/3 <111> interstitial loops, suggesting that the compressive stresses in this region are much less. The loop growth sequence often observed in many different types of specimens is 'clusters' → a/3 <111> > loops → a/2 <110> loops. In the present work, on going from 650° to 950°C, the number of atoms comprising the a/3 <111> and a/2 <110> loops in the two damage layers progressively changed. For the second damage layer, the relative number of atoms in the a/2 <110> loops increased by ~4x, while for the first damage layer, the corresponding increase was very much less.

At 1050°C, the loops in the second damage layer had completely annealed out, while those in the first damage layer were still present. Furthermore, for the first damage layer, the relative number

of atoms in the a/2 <110> loops compared with the a/3 <111> loops had increased to ~20x, and the total number of atoms in the two kinds of loops was now ~13x greater than the number of implanted ions. The stacking fault tetrahedra also increased markedly in size and number (data Table 2).

II. Defects-Electrical-SIMS-Diffraction Contrast Correlations

In order for a P atom to become electrically active in the Si lattice, it should occupy a substitutioned site in the lattice. On subsequent annealing, high electrical activity will be possible if vacant sites are available to the P atoms. At a given annealing temperature an equilibrium concentration of vacancies will be present throughout the material. However, the concentration of vacancies will be higher near the surface as described above. Therefore, a large fraction of P atoms should be expected to occupy substitutional sites in the region between the surface and the first damage layer contributing to higher electrical activity in this region. In the deeper parts, the thermal vacancies are expected to be uniformly distributed. However, in the region containing the layers of interstitial dislocation loops, the electrical activity may be mainly determined by the interaction of P atoms and vacancies with the dislocation cores. The inside/outside experiments indicate that a large fraction of the P atoms are bound up with the dislocation cores. Small interstitial loops are also effective sinks for vacancies. Therefore, reduced electrical activity is expected near the damage layers. Below the damage layers higher carrier concentration is

expected because the P atoms will be able to combine with the thermal vacancies. This is in agreement with the experimental observations. The carrier concentration values in the profiles probably do not represent the absolute magnitudes because this requires several correction factor that are difficult to estimate due to the complicated distribution of carriers, the damage present and the depths resolution of the measurement technique. However, the shape of the profiles is expected to be qualitatively representative.

In summary, the recrystallization behaviour of a buried amorphous layer in ion implanted (111) Si has been discussed. It was found that the recrystallization began simultaneously at both upper and lower amorphous/crystalline interfaces. The amorphous to single crystal transformation was slow up to 550°C but increased rapidly above 550°C. At 750°C or above, two discrete secondary damage layers with each containing dislocation loops, were formed. The dislocation loops in both layers were interstitial in nature; however, the habit planes of the loops in the two layers were different. This was assumed to be associated with the different magnitude of the biaxial compressive stresses at the two damage regions.

By combining the TEM results with those obtained by the SIMS and Hall measurements, it was found that strong correlations existed between the structural, compositional and electrical results. It was revealed that pronounced segregation of P atoms occurs near the defect layers and that a large fraction of the P atoms were bound up with the defect layers, probably occupying special cyrstallographic sites near

the dislocation cores. Such damage-impurity interaction reduced the electrical activity.

From the practical point of view, the first damage layer is probably more important, because pronounced reduction in the electrical activity occurs in this region. The second damage layer could also be important if it occurred within the depletion region of the p-n junction formed.

ACKNOWLEDGEMENTS

The authors gratefully acknowledge the help of Dr. J. Titchmarsh of AERE Harwell (England) for taking the convergent beam diffraction patterns, and C. W. Magee of RCA labs (USA) for taking the SIMS measurements, included in the manuscript. The TEM work described in the text was performed at the University of Oxford (England). Financial support of the work in part came through the Science Research Council (UK), and in part through the Director, Office of Energy Research, Office of Basic Energy Sciences, Materials Science Division of the U. S. Department of Energy under contract No. DE-AC03-76SF00098.

REFERENCES

Bicknell, R. W., 1973, J. Microscopy 98, 165.

Chadderton, L. T., 1965, Radiation Damage in Crystals, John Wiley and Sons, Inc., pp. 82.

Chadderton, L. T. and Eisen, F. H., 1971, Rad. Eff. 7, 127.

Cottrill, R. M. J., 1961, Phil., Mag., 6 1351.

Crowder, B. L. and Title, R. S., 1970, Proc. Int. Conf. Ion Imp. Thousand Oaks, Rad. Eff.

Csepregi, L., Mayer J. W., and Sigmon, T. W., 1975, Phys. Lett. 54A, 157.

Cspregi, L., Kennedy, E. F., Lau, S. S., Maye J. W., and Sigmon, T. W., 1976, App. Phys. Lett. 29, 646.

Csepregi, L., Kennedy, E. F., Gallagher, T. J., Mayer, J. W. and T. W. Sigmon, 1977, J. App. Phys. 48 4234.

Davidson, S. M. and Booker, G. R., 1970, Rad. Eff. 6 33.

Davidson, S. M., 1972, J. Phys. E. 5, 23.

Drosd, R. and Washburn, J., 1980, J. App. Phys. 51, 4106.

Drosd, R. and Washburn, J., 1982, J. Appl. Phys. 53, 397.

Fletcher, J. and Booker, G. R., 1978, 9th International Conference on Electron Microscopy (Toronto) 1, 364.

Gerasimov, A. T., Zorin, E. I., Paulov, P. V. and Tetelbaum, D. I., 1972, Phys. Stat. Solidi. 12 679.

Hirsch, P. B., Howie, A., Nicholson, R. B., Pashley, D. W., and Whelan, M. J., 1965, Electron Microscopy of thin crystals, (Butterworths, London).

Jenkins, M. L., Cockayne, D. J. H., and Whelan, M. J., 1973, J. Microsc. 98, 155.

Komarov, F. F., Soloviyer, V. S. and Shiryayer, S. Yu, 1979, Rad. Eff. 42, 169.

Lau, S. S., 1978, J. Vac. Sci. Tech. 15, 1656.

Madden, P., 1974, Ph.D. Thesis, Oxford University.

Magee, C. W., 1979, J. ELectrochem. Soc. 126, 660.

Masters, B. J., Fairfield, J. M. and Crowder, B. L., 1970, Rad. Eff. 6, 57.

Pettit, H. R. and Booker, G. R., 1977, Conf. Series. Inst. Phys. (London) 10, 290.

Ray,I. L. F. and Cockayne, D. J. M., 1970, Phil. Mag. 22 853.

Sadana, D. K., Fletcher, J. and Booker, G. R., 1977, Elec. Lett. 13, 632.

Sadana, D. K., to be published.

Saldin, D. K., Stathopoules, A. Y., and Whelan, M. J., 1979, Phil. Trans. 292, 523.

Silcox, J. and Hirsch, R. B., 1959, Phil. Maj. 72.

Spaepan, F., 1978, Acta. Met. 26, 1167.

Tseng, W. T., Liau, Z. L., Lau, S. S., Nicolet, M-A. and Mayer, J. W., 1976, Thin Solid Films 46.

Washburn, J., 1980, Defects in semiconductors 2, Proc. Materials Research. Society Meeting, p. 209.

Table 1. Width of the buried amorphous layer as a function of annealing temperature.

ANNEALING TEMP. (°C)	DEPTH (Upper Edge) (Å)	DEPTH (Lower Edge) (Å)	WIDTH OF DAMAGE BAND Å	MEAN DEPTH (DAMAGE CLUSTERS) (Å)
RT	600	1950	1350	----
400	750	1670	920	----
550	750	1500	750	2250

Table 2. Comprehensive TEM analysis data from individual layers of the dislocation loops.

		LAYER S				LAYER T		
ANNEALING TEMP (°C)	MEAN DEPTH (Upper Layer) (Å)	a/2 <110> Loops density, mean dia., nature	a/3 <111> Loops density, mean dia. nature (parallel)	S.F.T.s. density, mean dia., nature	MEAN DEPTH (Lower Layer) (Å)	a/2 <110> Loops density, mean dia. nature	a/3 <111> Loops density, mean dia. nature (inclined)	a/3 <111> Loops density, mean dia. nature (inclined)
750	1200	$1.8 \times 10^{10}/cm^2$, 600 Å, Interstitial	$9.0 \times 10^{9}/cm^2$, 400 Å, Interstitial	$7.5 \times 10^{9}/cm^2$ ~100 Å Vacancy	2000	$1.1 \times 10^{10}/cm^2$ 250 Å, Interstitial	$\sim 10^{10}/cm^2$ 250 Å Interstitial	$\sim 10^{10}/cm^2$ 250 Å Intestitial
850	1070	$1.3 \times 10^{10}/cm^2$, 800 Å, Interstitial	$9.0 \times 10^{0}/cm^2$ 600 Å, Interstitial	$1.5 \times 10^{9}/cm^2$, ~100 Å Vacancy	1730	$7.2 \times 10^{9}/cm^2$ 250 Å, Interstitial	$1.5 \times 10^{10}/cm^2$, 250 Å Interstitial	$\sim 10^{10}/cm^2$, 250 Å, Interstitial
950	1070	$5.4 \times 10^{9}/cm^2$, 1000 Å, Interstitial	$4.3 \times 10^{9}/cm^2$, 800 Å, Interstitial	$1.5 \times 10^{9}/cm^2$, ~100 Å Vacancy	2100	$2.0 \times 10^{8}/cm^2$ 300 Å, Interstitial	$2.9 \times 10^{8}/cm^2$ 350 Å, Interstitial	$10^{8}/cm^2$ 350 Å, Interstitial
1050	1350	$2.7 \times 10^{9}/cm^2$ 1600 Å, Interstitial	$1.2 \times 10^{9}/cm^2$ 950 Å, Interstitial	$4.5 \times 10^{10}/cm^2$ ~ 100 Å Vacancy				

FIGURE CAPTIONS

Fig. 1. Schematic diagram illustrating the specimen preparation method used to investigate the damage in regions P, Q and R, respectively from an ordinary plan view specimen (a) cross-sectional view of the damage, (b) Cross-sectional view of the chemically thinned plan view specimen. TED from area A1 corresponds to region P, (c) Region P removed by ion-beam milling. TED from area B1 corresponds to region Q (amorphous layer), (d) TED from area C1 corresponds to region R.

Fig. 2. Schematic diagram illustrating the specimen preparation method used to investigate the damage in layers S and T, respectively from an ordinary plan view specimen. (a) Cross-sectional view of the damage, (b) Cross-sectional view of the chemically thinned plan view specimen, Areas A1 and A2 were used to study the damage layer S and above, (c) layer S removed by ion-beam milling. Area B2 was used to study the damage in layer T.

Fig. 3. TEM cross-section bright-field micrographs for (a) unannealed, (b) 400°C anneal and (c) 550°C anneal. The annealing was carried out in a nitrogen ambient for 20 min.

Fig. 4. Convergent beam micro-diffraction patterns from (a) region P, (b) region Q and (c) region R. The absence of the diffraction spots in region Q indicates that the material is amorphous in this region.

Fig. 5. TEDs as a function of depth for an unannealed specimen (a) TEDs from areas A1 (left side) and A2 (right side), (b) TEDs from area B1 (left side) and B2 (right side), (c) TED from area C1. All micrographs were takenwwwith bright-field diffraction contrast conditionins using a 220 type reflection.

Fig. 6. TEM micrographs from the specimen annealed at 650°C for 20 minutes in a nitrogen atmosphere (a) cross-sectional view (b) plan view (includes layers S and T).

Fig. 7. TEM micrographs from the specimen annealed at 750°C for 20 minutes in a nitrogen atmosphere (a) cross-sectional view, (b) plan view of layers, (c) plan view of layer T.

Fig. 8. TEM micrographs from the speicmen annealed at 850°C for 20 minutes in a nitrogen atmosphere (a) cross-sectional view, (b) plan view of layer S (c) plan view of layer T.

Fig. 9. TEM micrographs from the specimen annealed at 950°C for 20 minutes in a nitrogen atmosphere (a) cross-sectional view, (b) plan view of layer S (c) plan view of layer T.

Fig. 10. TEM micrographs from the specimen annealed at 1050°C for 20 minutes in a nitrogen atmosphere (a) cross-sectional view, (b) plan view of layers S.

Fig. 11. Phosphorus distribution curve from the 650°C annealed sample. The curve corresponds to the TEM specimen of Fig. 7.

Fig. 12. Phosphorus distribution curve from the 750°C annealed sample. The curve corresponds to the TEM specimen of Fig. 8.

Fig. 13. Phosphorus distribution curve from the 850°C annealed sample. The curve corresponds to the TEM specimen of Fig. 9.

Fig. 14. Phosphorus distribution curve from the 950°C annealed sample. The curve corresponds to the TEM specimen of Fig. 10.

Fig. 15. TEM +g and -g bright-field micrographs from the same area of the 750°C annealed sample using a 220 type reflection.

Fig. 16. TEM -g and -g bright-field micrographs from the same area of the 850°C annealed sample using a 220 type reflection.

Fig. 17. TEM +g and -g bright-field micrographs from the same area of the 950°C annealed sample using a 220 type reflection.

Fig. 18. Carrier concentration (n) and mobility (μ_r) profiles obtained from the sample of Fig. 9.

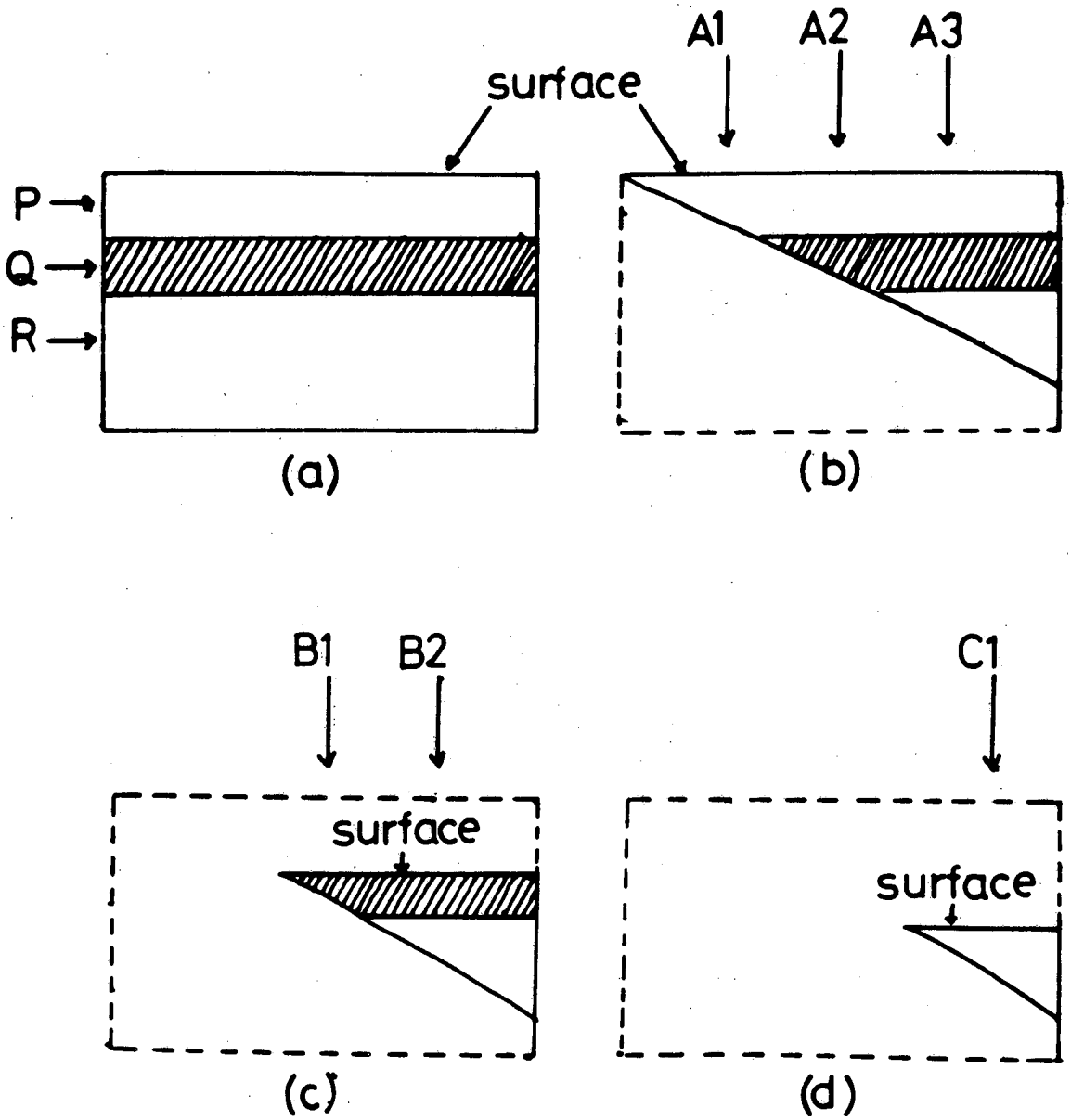

Fig. 1

XBL 805-9665

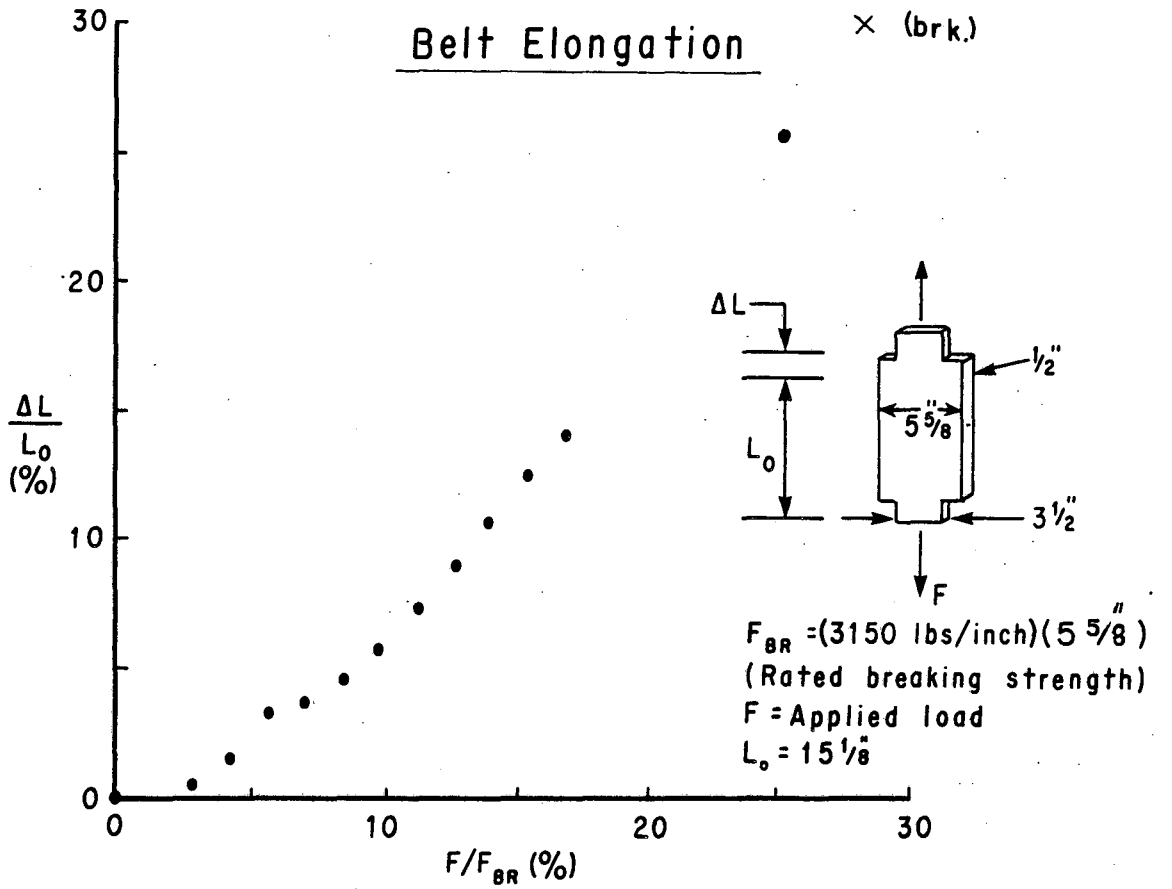

Fig. 2

XBL 805-9666

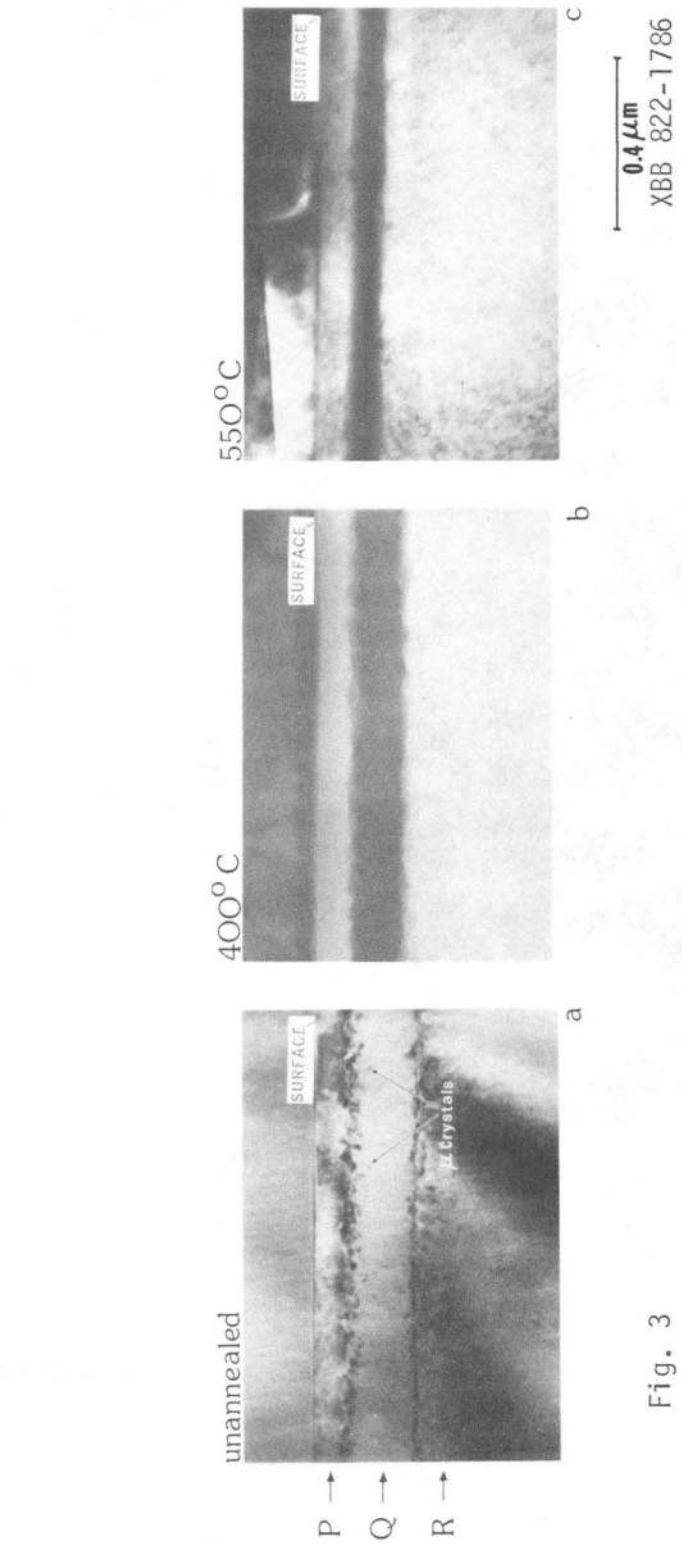
unannealed
400°C
550°C
SURFACE
SURFACE
SURFACE
μ Crystals
P
Q
R
a
b
c
0.4 μm
XBB 822-1786

Fig. 3

Unannealed Cross-Section

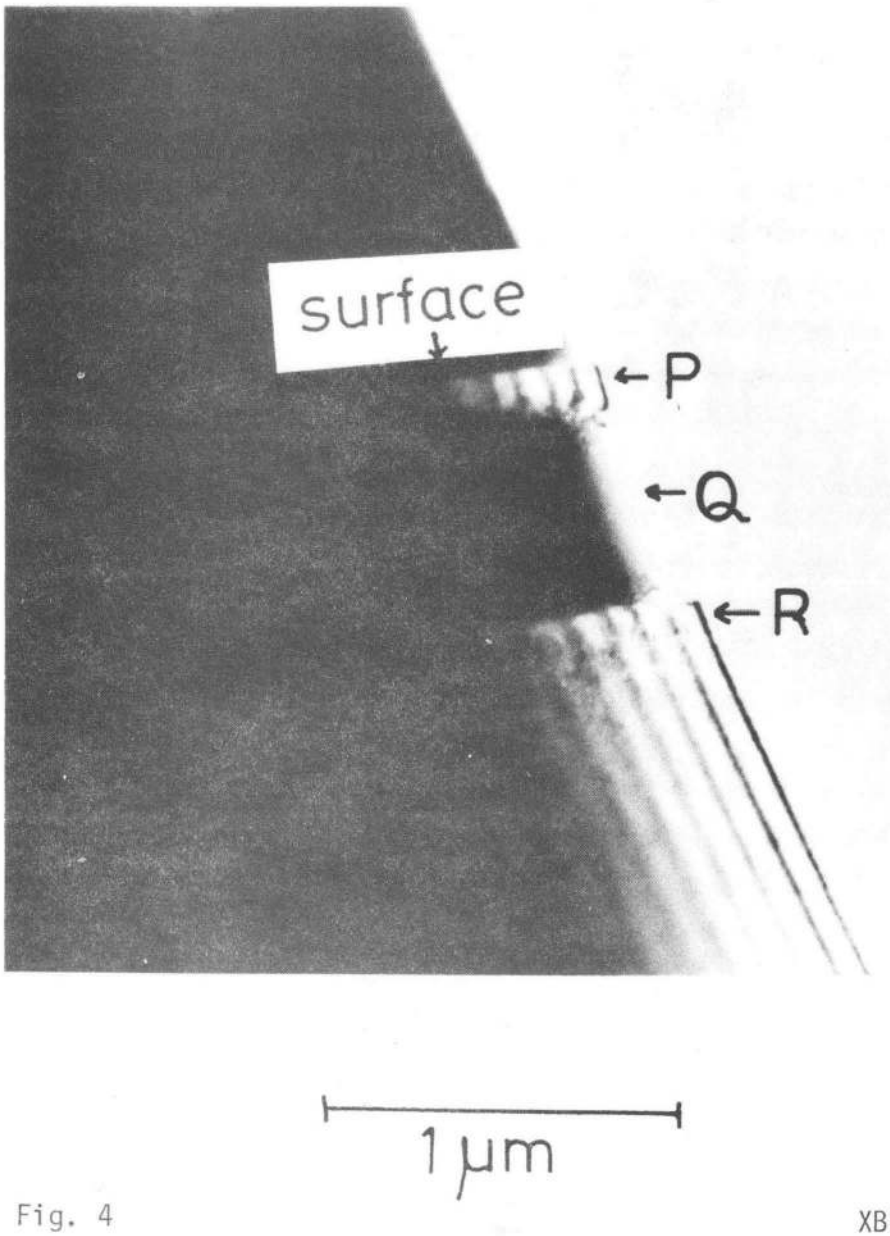

Fig. 4

XBB 805-6379

Convergent Beam Micro-Diffraction Patterns

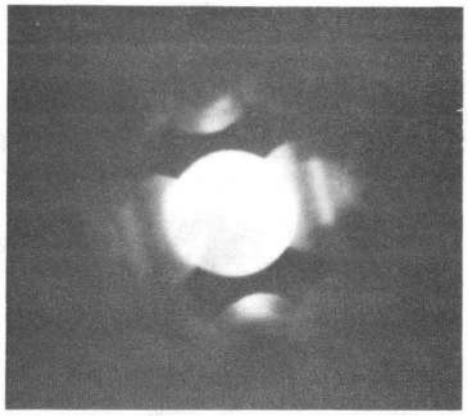

(a)

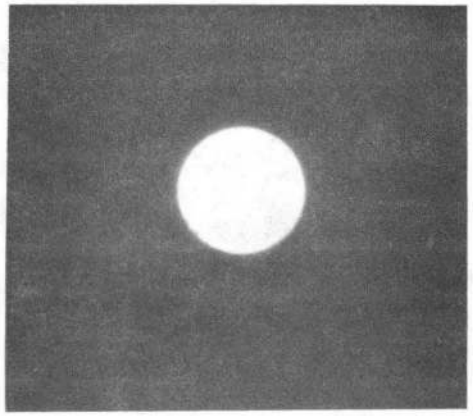

(b)

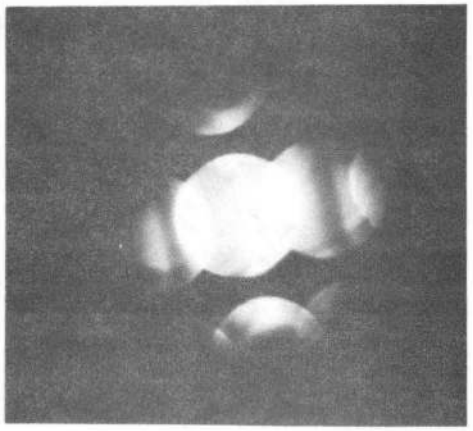

(c)

Fig. 5 XBB 805-6382

Diffraction Patterns as Function of Depth

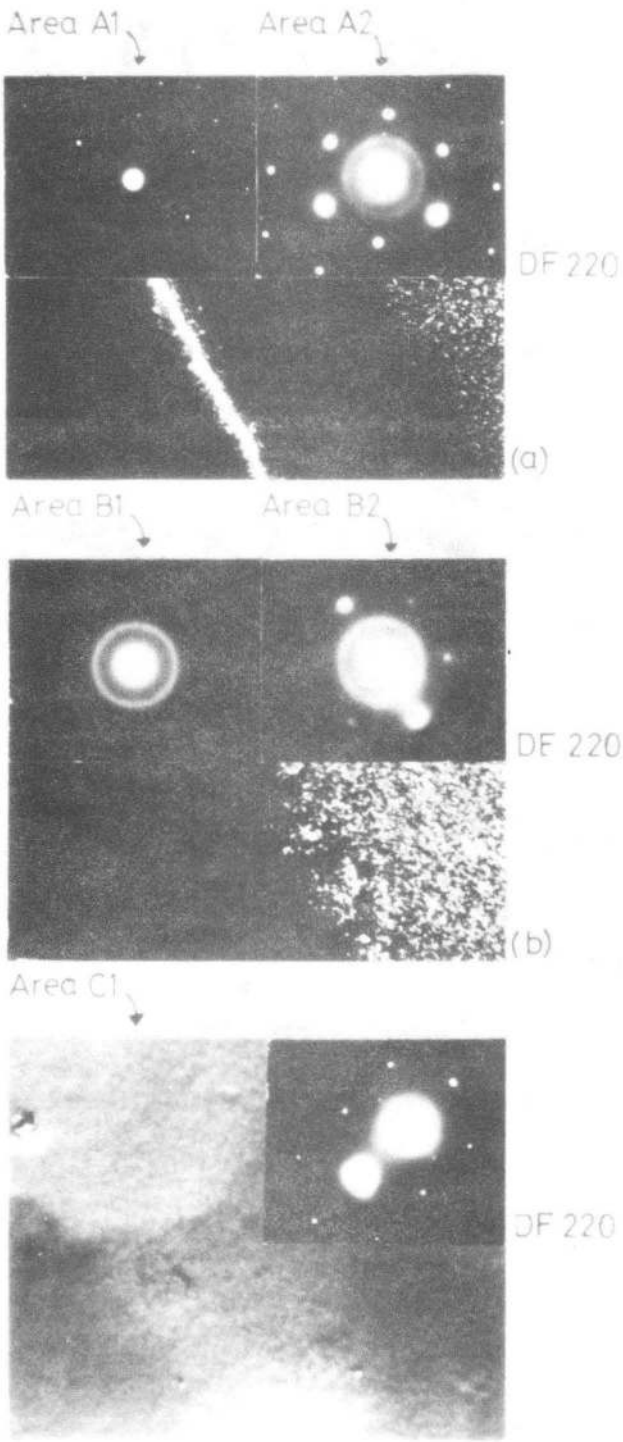

Fig. 6 XBB 805-5900

Annealing Temp = 650°C

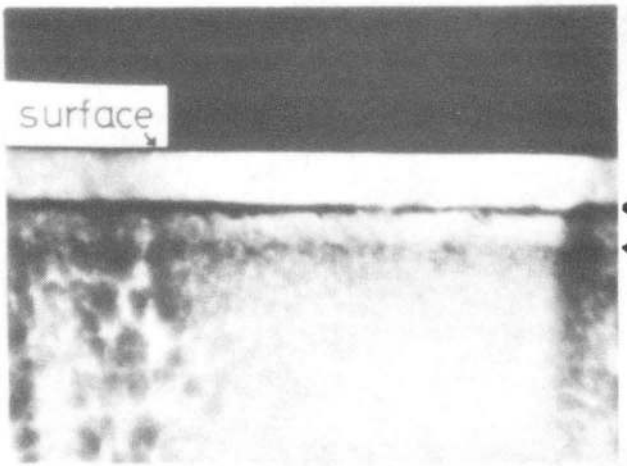

(a)

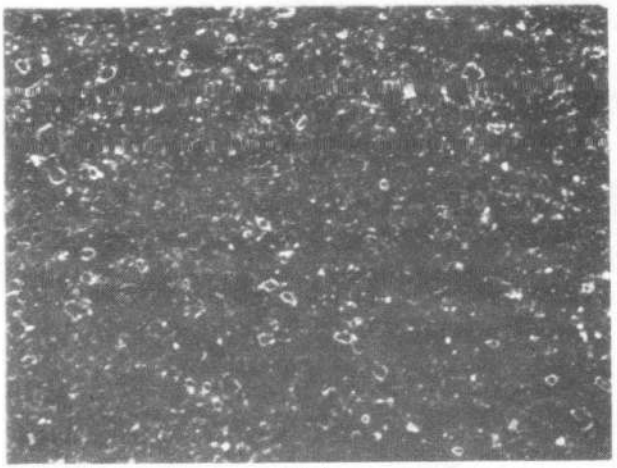

(b)

Fig. 7

XBB 827-6396

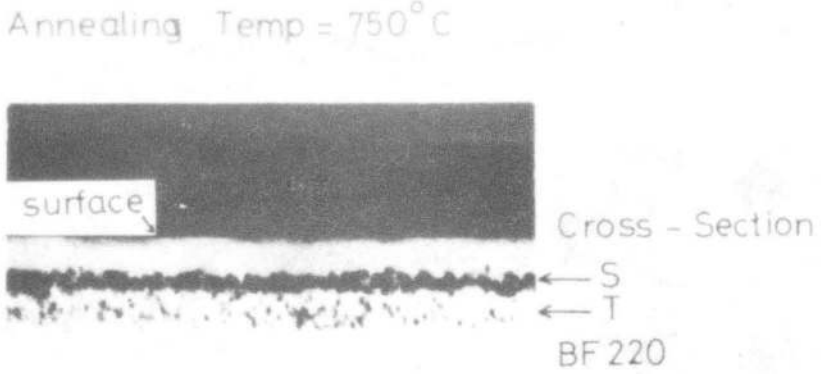

(a)

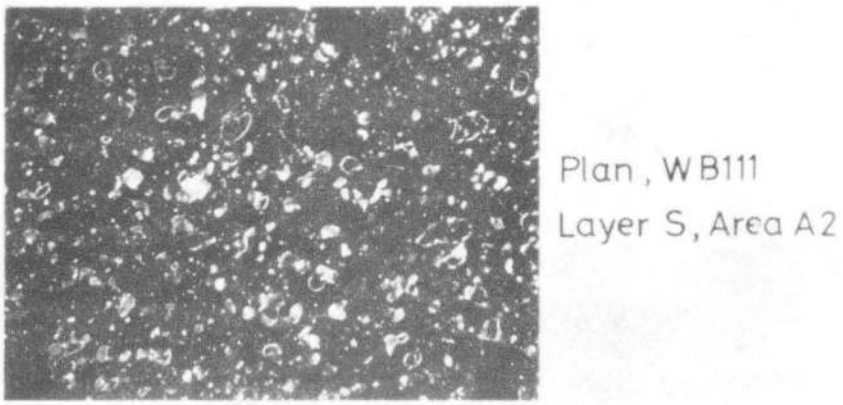

(b)

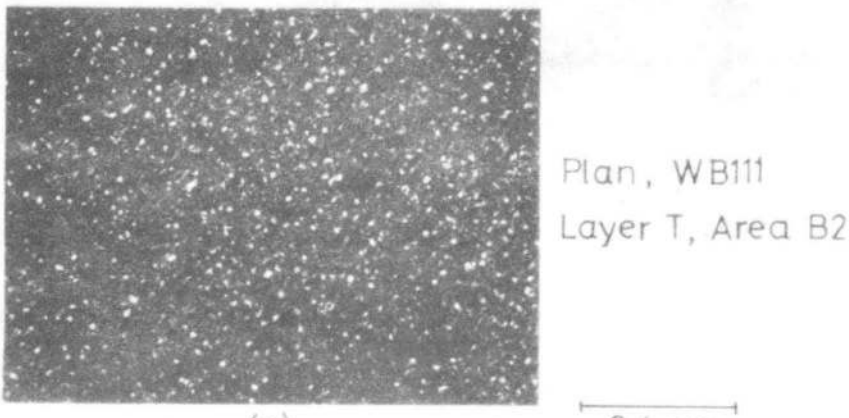

(c)

Fig. 8

XBB 825-4380

Annealing Temp = 850° C

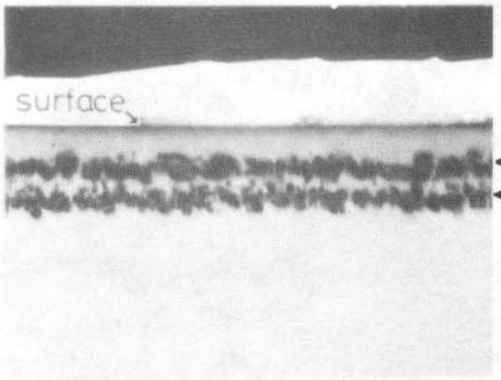

(a)

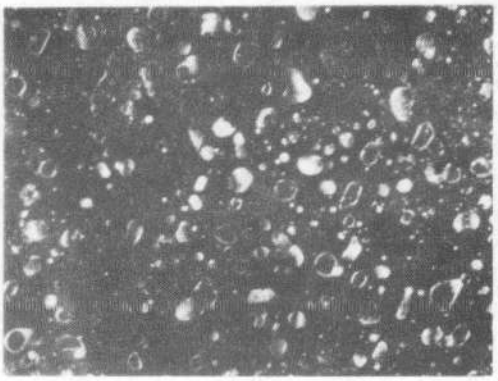

(b)

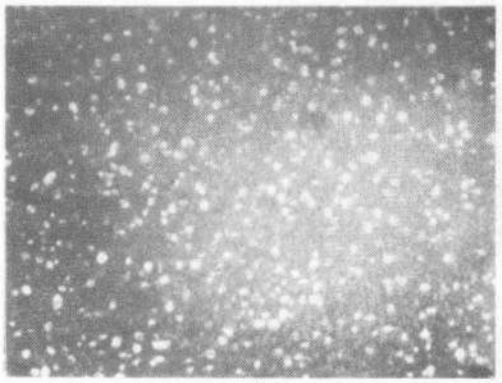

(c)

Fig. 9

XBB 827-6398

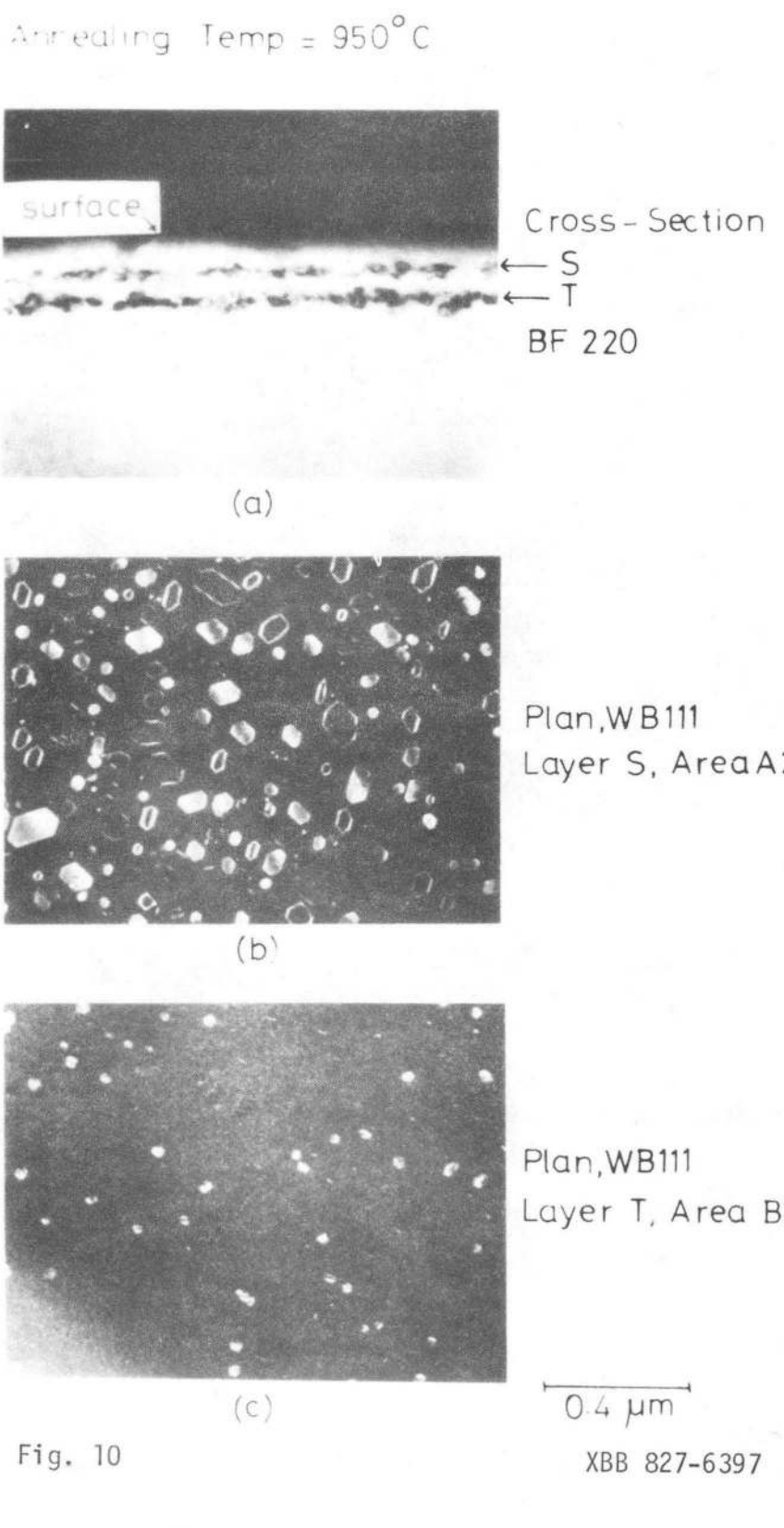

Fig. 10

XBB 827-6397

Annealing Temp = 1050° C

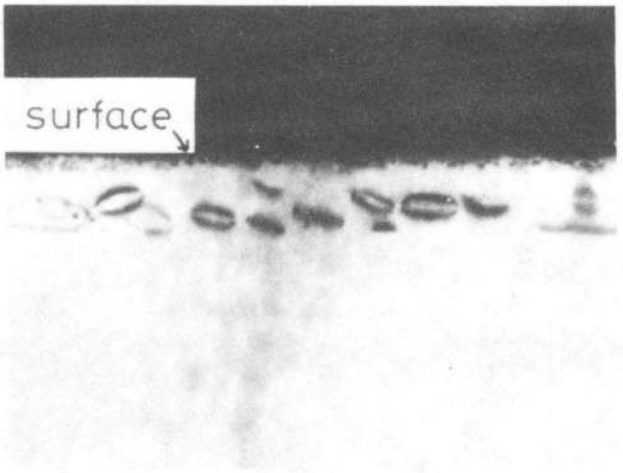

Cross -Section
←S
BF 220

(a)

Plan, WB111
Layer S, Area A2

0.4 μm

(b)

Fig. 11

XBB 805-6380

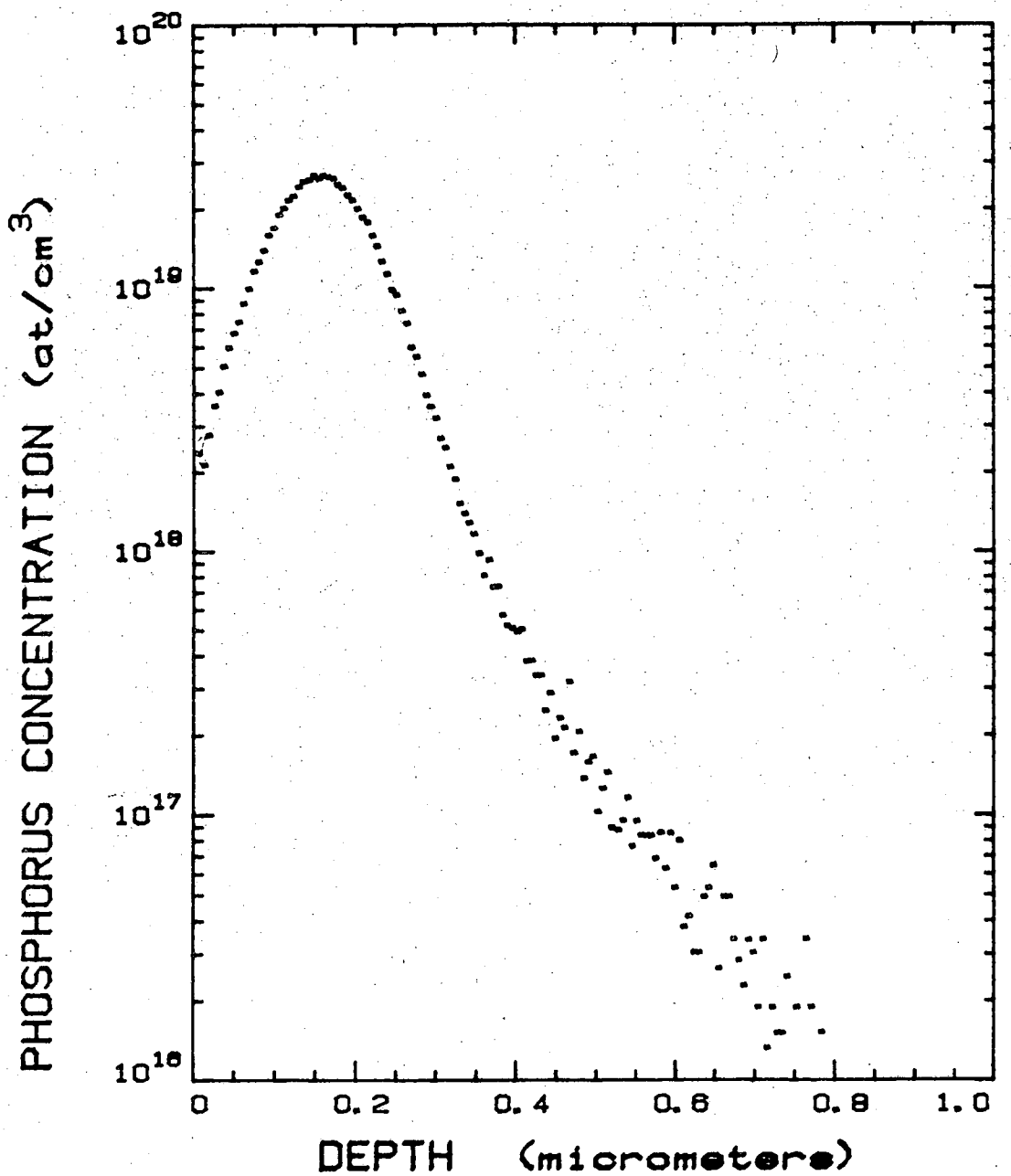

Fig. 12

XBL 823-8330

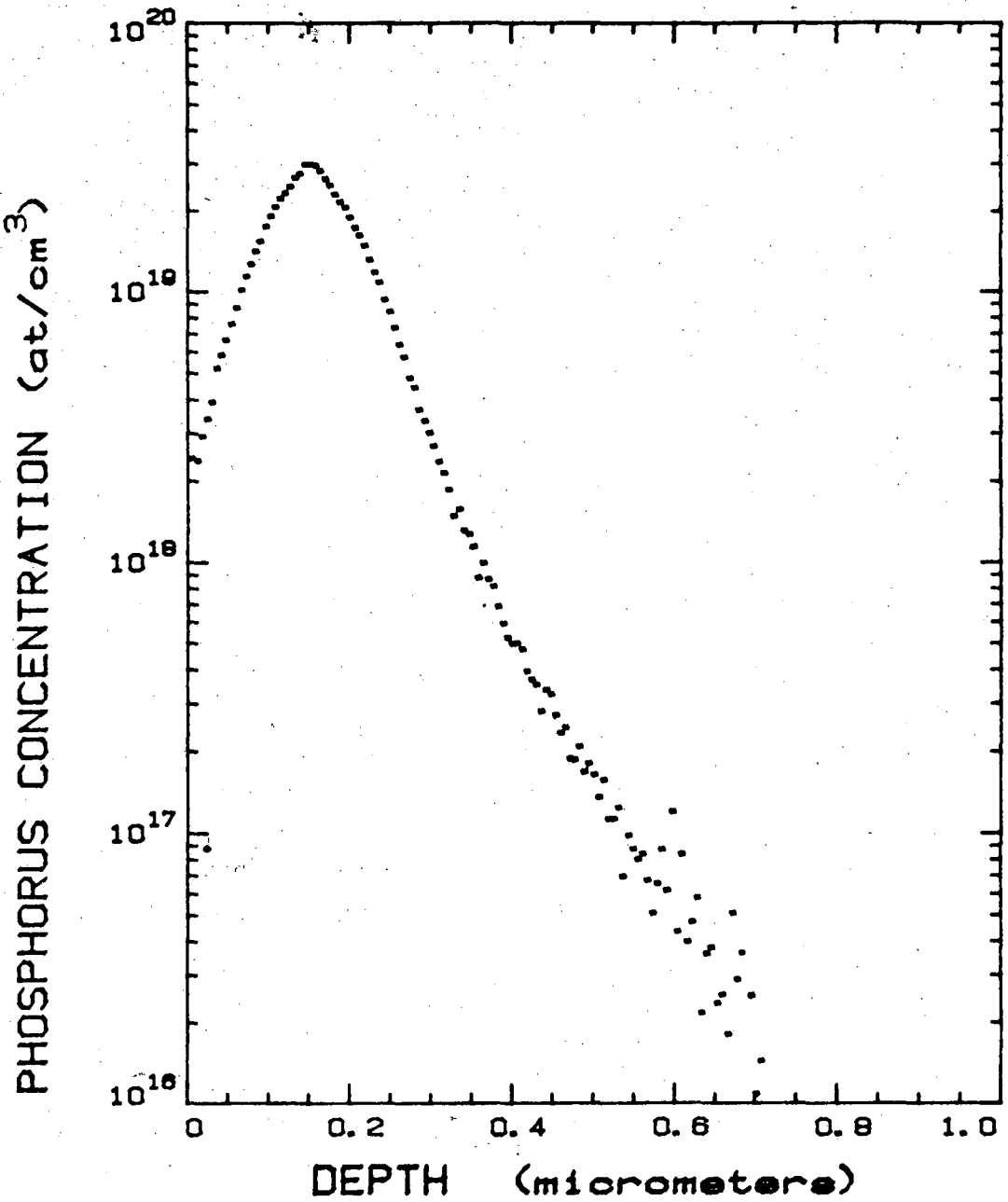

Fig. 13

XBL 823-8329

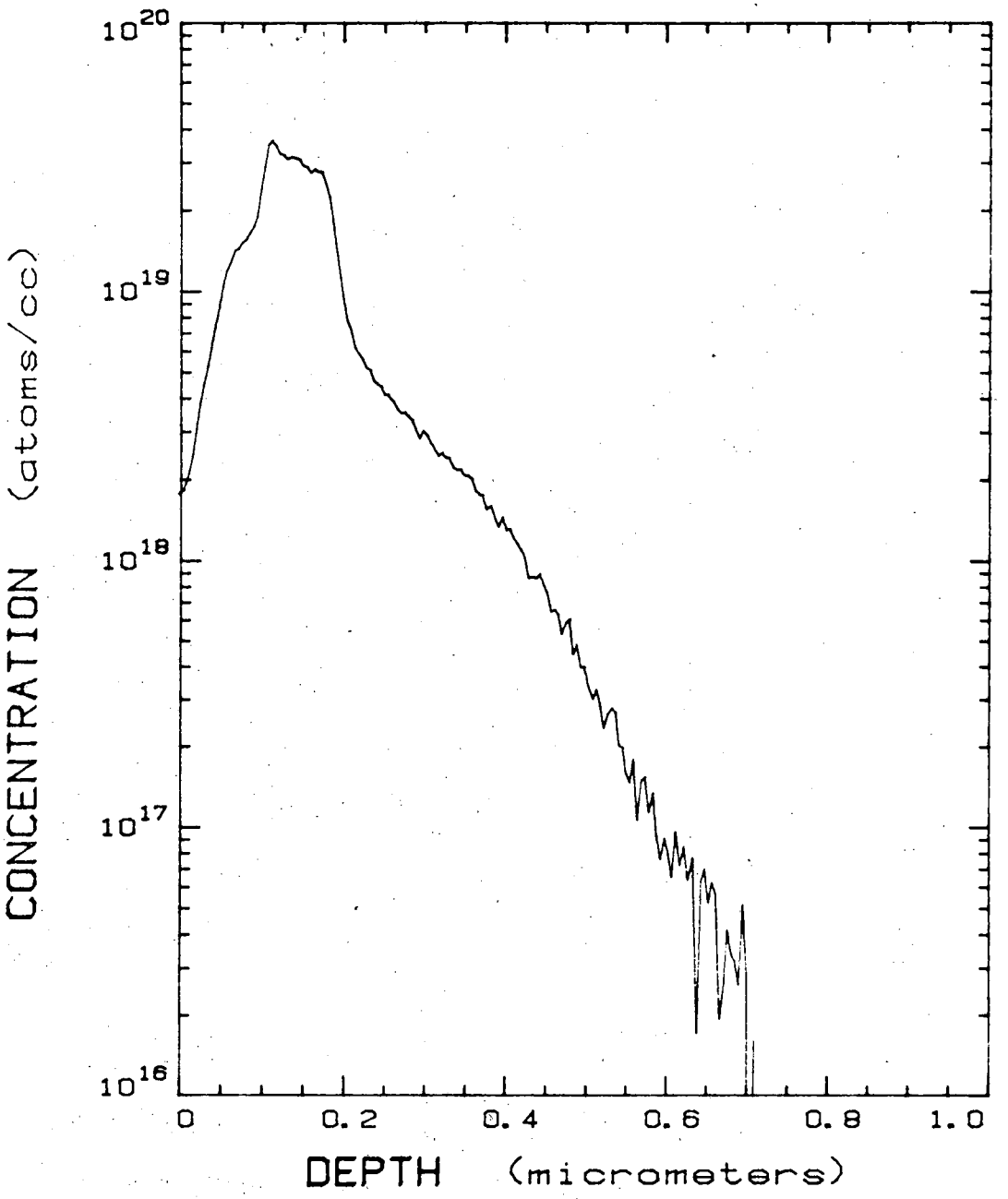

Fig. 14

XBL 823-8331

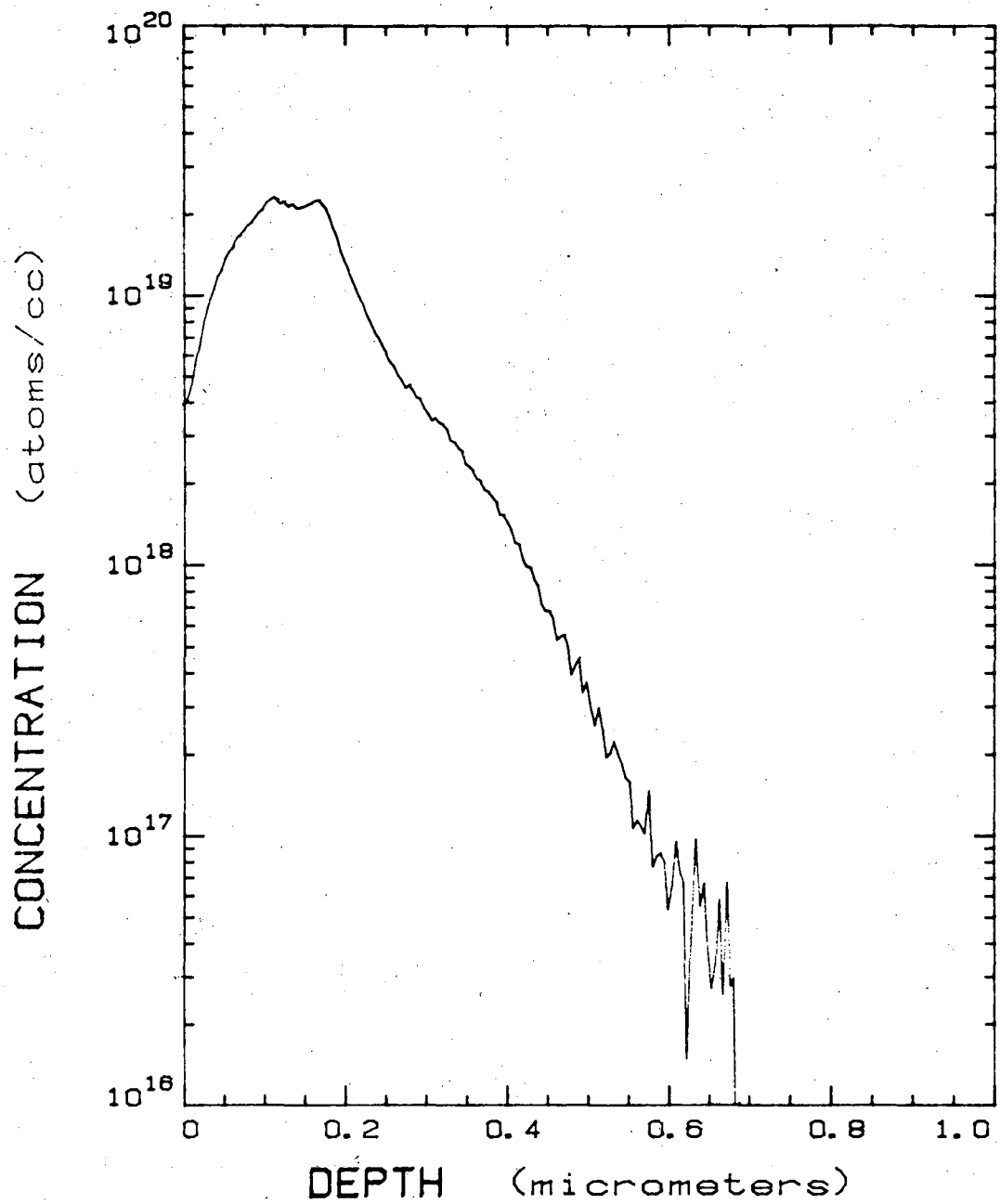

Fig. 15

XBL 823-8328

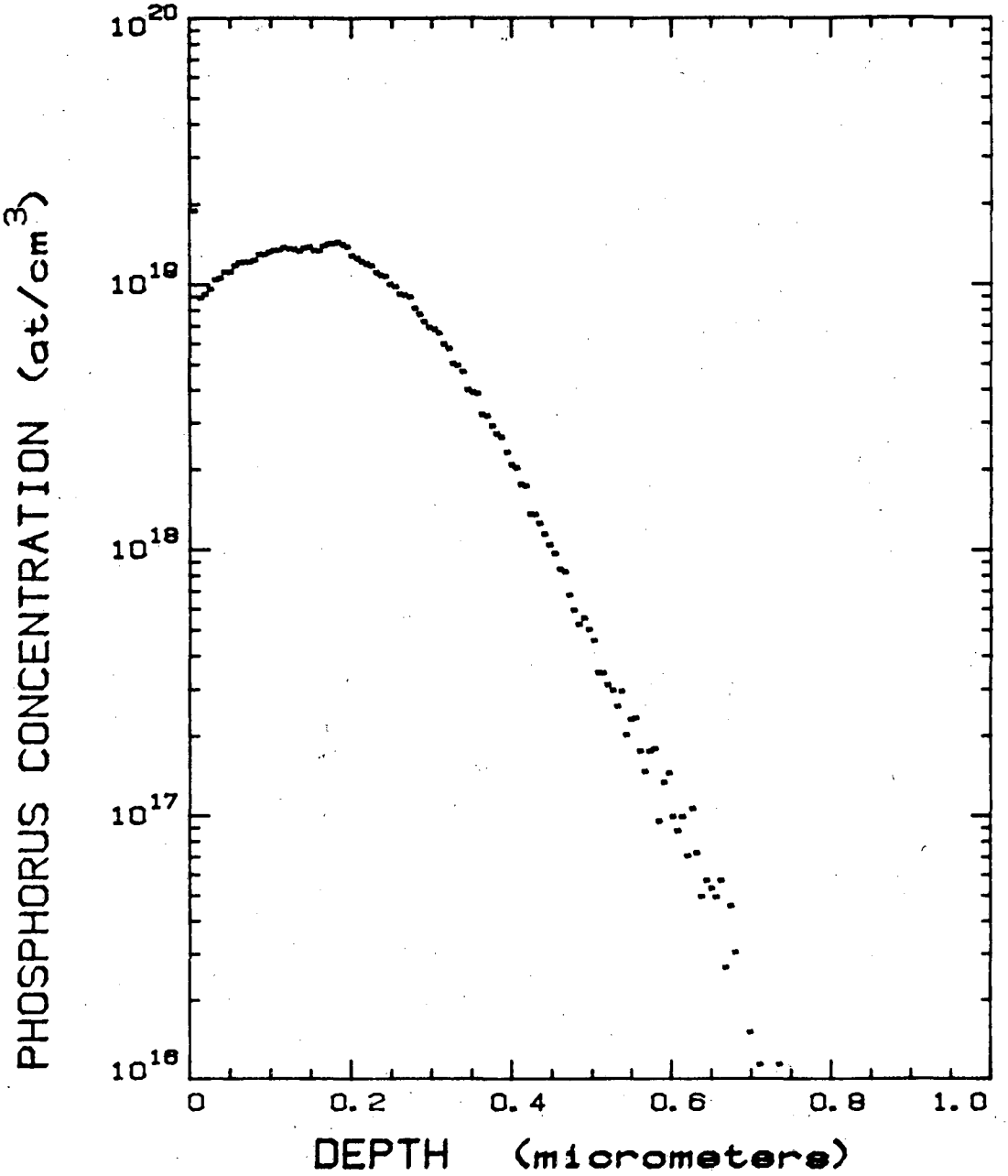

Fig. 16

XBL 823-8327

750°C

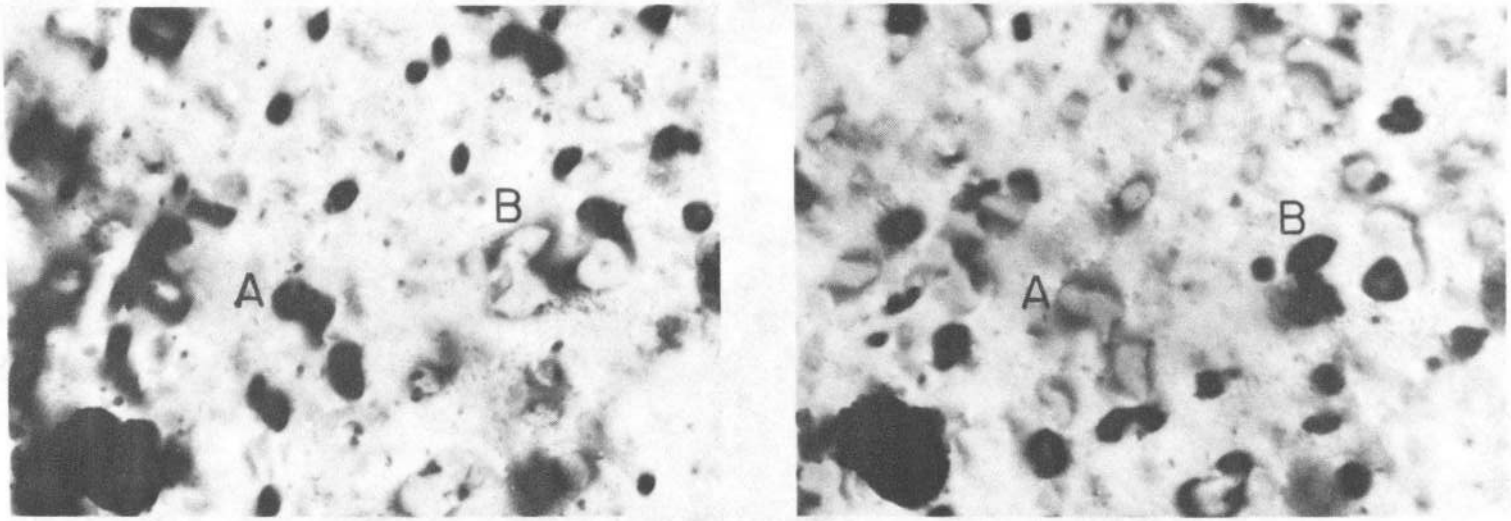

+g -g

Fig. 17

XBB 803-3269

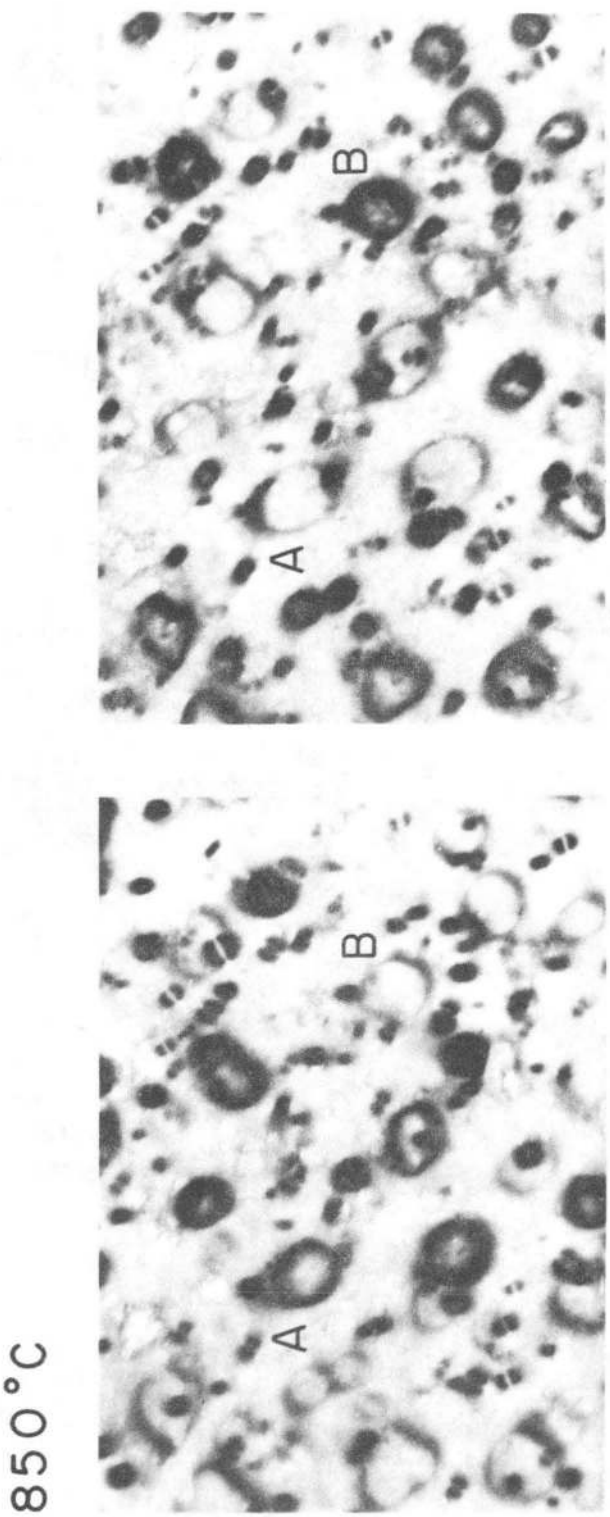

XBB 803-3268

Fig. 18

950°C

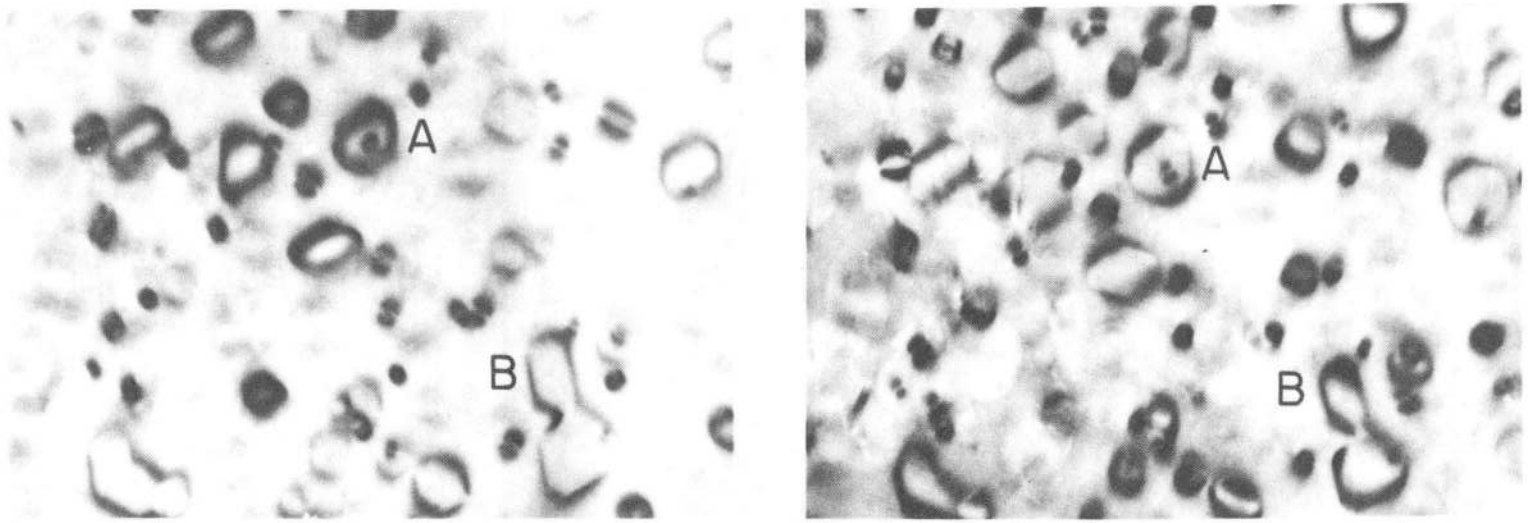

+g -g

Fig. 19

XBB 803-3267

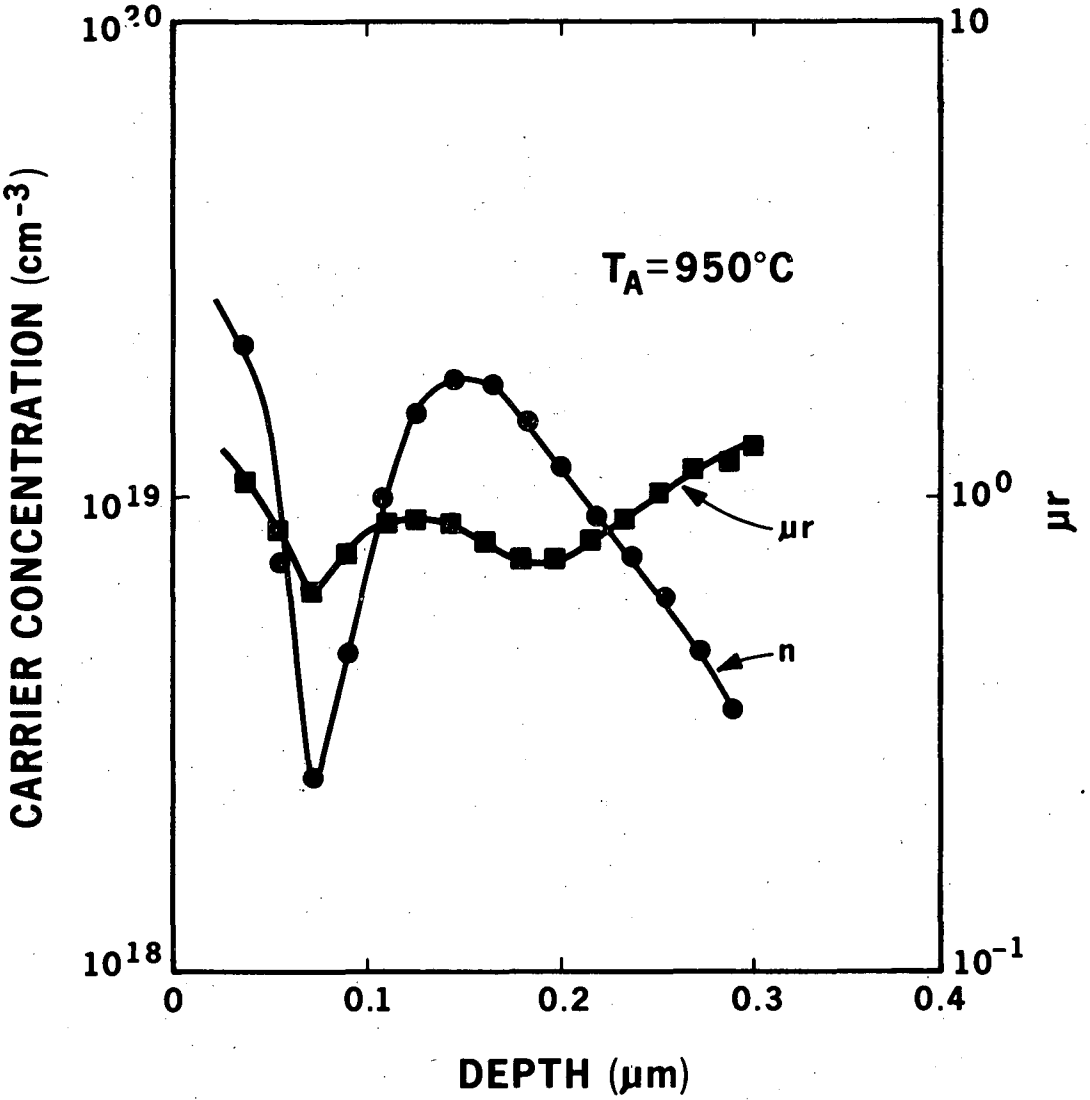

Fig. 20

XBL 823-8151

TECHNICAL INFORMATION DEPARTMENT
LAWRENCE BERKELEY LABORATORY
UNIVERSITY OF CALIFORNIA
BERKELEY, CALIFORNIA 94720